Resubmitted to Acta Mechanica in March 2021

Propagation of conductive crack along interface of piezoelectric/piezomagnetic bimaterials

P. Ma[1,2] , R.K.L. Su[1,*], W.J. Feng[3]

[1] *Department of Civil Engineering, The University of Hong Kong, Hong Kong, PR China*

[2] *Bureau of Public Works of Pingshan District, Shenzhen, PR China*

[3]*Department of Engineering Mechanics, Shijiazhuang Tiedao University, Shijiazhuang 050043, PR China*

Abstract

This paper investigates the fracture characteristics of a Yoffe conductive crack moving along the interface of piezoelectric (PE)/piezomagnetic (PM) bimaterials. By assuming that the tangential electric- and magnetic- fields along the crack surface is zero and that the speed of the moving crack is less than the minimum shear wave speed of the bimaterial system, the considered problem can be transformed into a Riemann-Hilbert boundary value problem of vector form. Then the singularity parameters are exactly solved for different speed regions. In contrast to the anti-plane moving crack model including impermeable and permeable crack-face assumptions along the interface of magnetoelectroelastic (MEE) bimaterials studied before, which shows inverse square-root singularity, three novel kinds of singularities are found as the speed of the moving crack is varied for the present PE/PM interface model, which can be defined as $\delta_{1,2} = -1/2 \pm i\varepsilon$ (Case 1), $\delta_{1,2} = -1 \pm i\varepsilon$ (Case 2) and $\delta_{1,2} = -1/2 \pm \kappa$ (Case 3), and the third parameter $\delta_3 = -1/2$ always holds true for all three cases. Two bimaterial combinations, i.e., $BaTiO_3/CoFe_2O_4$ and $BaTiO_3$/Terfenol-D, are numerically examined. Different from the piezoelectric case, Case 3 does not appear for $BaTiO_3/CoFe_2O_4$ bimaterial combination. Above

* Corresponding author. Tel: +852 2859 2648, fax: +852 2559 5337 (R.K.L. Su);
E-mail address: mapengsjz@163.com (P. Ma); klsu@hku.hk (R.K.L. Su); wjfeng9999@126.com (W.J. Feng).

all, the singularity parameters significantly depend on the speed of the moving crack and the material properties of bimaterial systems.

Keywords: Moving conductive crack; Interface crack; Piezoelectric/piezomagnetic bimaterial; Oscillating singularity; Speed region

1. Introduction

Piezoelectric (PE)/piezomagnetic (PM) layered materials, have attracted increasingly more attention as they are technologically simple to manufacture and high ME (magnetoelectrical) coefficients can be obtained [1]. However, cracks usually develop at the interface of the PE/PM layered materials during their servicing and thus their fracture analyses have received much attention recently [2-6].

In practical engineering, dynamic interface cracks and their propagation are more problematic. An important topic of dynamic fracture mechanics is moving cracks [7], where a crack with fixed length to move inside a material. This crack model does not exist in reality, however, under the assumption of a moving crack with fixed length, the analytical solution is available and this is critical to help us cognize the singularity of the generalized stresses in the vicinity of crack tip and obtain some dynamic information around the crack tip, for example crack deflection [8]. And the moving crack model has also been extended to analyzing the fracture behaviors of magnetoelectroelastic (MEE) bimaterials [9-12]. Among them, Zhong and Li [9] studied a moving anti-plane Yoffe crack on the interface of MEE bimaterial based on magneto-electrically limited permeable crack-face conditions, in which the extended stresses possessed inverse square-root singularity. Hu et al. [11] investigated a magneto-electrically permeable moving Dugdale crack at the interface of an MEE bimaterial under anti-plane deformation, where the extended stresses are no longer singular. Ma et al. [12] examined the plane-strain problem of a moving crack with a contact zone at the interface of two dissimilar MEE materials

and evaluated the influence of the speed of the moving crack, poling direction and material volume fraction on the fracture parameters, where the extended stresses at crack tip also exhibited inverse square-root singularity owing to the presence of contact zone.

On the other hand, conductive cracks are very likely to form due to an extremely high local electric field through the crack, as well as due to electrode stratification or electrode-matrix debonding [13, 14]. For MEE materials, Tian and Rajapakse [15] investigated the static fracture behavior of conductive crack model in a homogeneous MEE material, and the extended stresses at crack tip had inverse square-root singularity as well. It is noted that although Ma et al. [16] considered the static behaviors of conductive interface crack in an MEE bimaterial, in their model only electrically conductive (i.e., magnetically permeable) assumption was adopted. In fact, for PE/PM layered materials, both electrically and magnetically conductive cracks may easily be developed at material interface due to complicated dynamic loading environment.

Wang and Zhong [17] investigated the problem of a Yoffe-type conducting crack moving with a constant velocity at the interface of two dissimilar piezoelectric half planes. However, to the best of our knowledge, the fracture problem of a moving conductive crack at the interface of a PE/PM bimaterial, which is actually a common layered material, has not been investigated yet. Therefore, in present study, this kind of crack model is put forward. Of importance, the crack-tip singularity characteristics of the novel model are detailed analyzed and discussed. The modeled crack singularities in this study completely differ from those of either an anti-plane impermeable or permeable crack moving along the interface of MEE bimaterials. The findings presented here should contribute to advancing current understanding of the failure behavior of PE/PM bimaterials. Moreover, the methodology employed in this paper can also be applied to the problems related to Maxwell stress and/or imperfect interface in the dissimilar piezoelectric and piezoelectric/piezomagnetic solids [18-21].

2. Basic relations for PE/PM bimaterial based on moving coordinate system

Consider a crack with a fixed length of 2a moving at a constant velocity V along the interface between the upper and lower half planes, which are PE and PM solids, respectively, as shown in Fig. 1. Both solids are transversely isotropic with the poling direction parallel to the x_3-axis. The bimaterial is loaded by the anti-plane shear stress σ_0 as well as in-plane electric field E_0 and magnetic field H_0 parallel to crack line at infinity. For the complexity of mathematics and physics involved, the speed of the moving crack is assumed to be less than the minimum shear wave speed of the bimaterial system. The constitutive equations (i.e., Eq. (1)) and the governing field equations (i.e., Eq. (2)) of the present model can be, respectively, written as follows,

for PE materials,

$$\begin{Bmatrix}\sigma_{32}\\ D_2\\ B_2\end{Bmatrix}=\begin{bmatrix}c_{44} & -e_{15} & 0\\ e_{15} & \alpha_{11} & d_{11}\\ 0 & d_{11} & \mu_{11}\end{bmatrix}\begin{Bmatrix}w_{,2}\\ E_2\\ H_2\end{Bmatrix},\quad \begin{Bmatrix}\sigma_{13}\\ D_1\\ B_1\end{Bmatrix}=\begin{bmatrix}c_{44} & -e_{15} & 0\\ e_{15} & \alpha_{11} & d_{11}\\ 0 & d_{11} & \mu_{11}\end{bmatrix}\begin{Bmatrix}w_{,1}\\ E_1\\ H_1\end{Bmatrix} \tag{1a}$$

and for PM materials,

$$\begin{Bmatrix}\sigma_{32}\\ D_2\\ B_2\end{Bmatrix}=\begin{bmatrix}c_{44} & 0 & -h_{15}\\ 0 & \alpha_{11} & d_{11}\\ h_{15} & d_{11} & \mu_{11}\end{bmatrix}\begin{Bmatrix}w_{,2}\\ E_2\\ H_2\end{Bmatrix},\quad \begin{Bmatrix}\sigma_{13}\\ D_1\\ B_1\end{Bmatrix}=\begin{bmatrix}c_{44} & 0 & -h_{15}\\ 0 & \alpha_{11} & d_{11}\\ h_{15} & d_{11} & \mu_{11}\end{bmatrix}\begin{Bmatrix}w_{,1}\\ E_1\\ H_1\end{Bmatrix} \tag{1b}$$

$$\sigma_{31,1}+\sigma_{32,2}=\rho\frac{\partial^2 w}{\partial t^2},\quad D_{1,1}+D_{2,2}=0,\quad B_{1,1}+B_{2,2}=0 \tag{2}$$

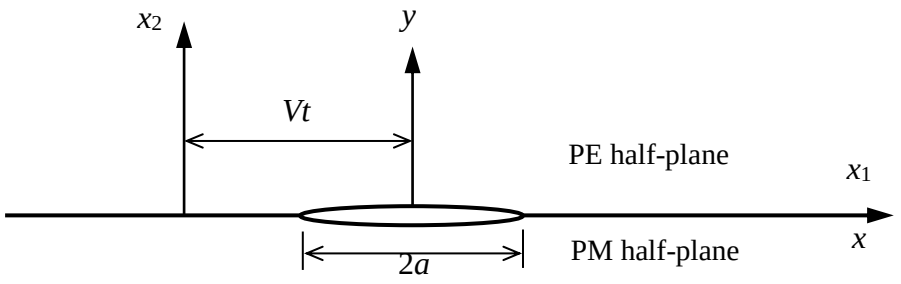

Fig. 1. Crack moving along interface between PE/PM materials

Correspondingly, the gradient equations are:

$$E_i = -\varphi_{,i}, \quad H_i = -\phi_{,i} \tag{3}$$

where σ_{ij}, D_i, and B_i are the components of the stresses, electric displacements and magnetic inductions, respectively; w, φ, and ϕ are the mechanical displacement, electric and magnetic potentials, respectively; and E_i and H_i are the electric and magnetic fields, respectively. c_{44}, e_{15}, h_{15}, and d_{11} are the elastic, PE, PM, and electromagnetic constants, respectively; α_{11} and μ_{11} are the dielectric permittivity and magnetic permeability, respectively, and ρ is the material density.

For convenience of the following calculations, two functions Ψ and Φ defined in terms of the electric displacements and magnetic inductions, respectively, are introduced as

$$D_2 = \Psi_{,1}, \quad D_1 = -\Psi_{,2}, \quad B_2 = \Phi_{,1}, \quad B_1 = -\Phi_{,2} \tag{4}$$

Using Eq. (4) and rearranging Eq. (1) results in:

$$\begin{Bmatrix} \sigma_{32} \\ E_1 \\ H_1 \end{Bmatrix} = \mathbf{E} \begin{Bmatrix} w_{,2} \\ -\Psi_{,2} \\ -\Phi_{,2} \end{Bmatrix} + \mathbf{F} \begin{Bmatrix} w_{,1} \\ \Psi_{,1} \\ \Phi_{,1} \end{Bmatrix}, \quad \begin{Bmatrix} \sigma_{31} \\ E_2 \\ H_2 \end{Bmatrix} = \mathbf{E} \begin{Bmatrix} w_{,1} \\ D_2 \\ B_2 \end{Bmatrix} + \mathbf{F} \begin{Bmatrix} w_{,2} \\ D_1 \\ B_1 \end{Bmatrix} \tag{5}$$

where

$$\mathbf{E} = \begin{bmatrix} E_{11} & 0 & 0 \\ 0 & E_{22} & 0 \\ 0 & 0 & E_{33} \end{bmatrix}, \quad \mathbf{F} = \begin{bmatrix} 0 & F_{12} & F_{13} \\ F_{12} & 0 & 0 \\ F_{13} & 0 & 0 \end{bmatrix} \tag{6}$$

and for PE materials,

$$E_{11} = c_{44} + \frac{e_{15}^2}{\alpha_{11}}, \; E_{22} = \frac{1}{\alpha_{11}}, \; E_{33} = \frac{1}{\mu_{11}}, \; F_{12} = -\frac{e_{15}}{\alpha_{11}}, \; F_{13} = 0 \tag{7a}$$

for PM materials,

$$E_{11}=c_{44}+\frac{h_{15}^2}{\mu_{11}},\ E_{22}=\frac{1}{\alpha_{11}},\ E_{33}=\frac{1}{\mu_{11}},\ F_{12}=0,\ F_{13}=-\frac{h_{15}}{\mu_{11}} \tag{7b}$$

It should be pointed out that the magnetic quantities associated with PE materials and the electrical quantities associated with PM materials are still considered because of dielectric permittivity α_{11} and magnetic permeability μ_{11} being nonzero.

Substituting Eq. (5) into Eq. (2) and using the relations $E_{2,1}=E_{1,2}$ and $H_{2,1}=H_{1,2}$ results in:

$$\nabla^2 w=\frac{1}{c_s^2}\frac{\partial^2 w}{\partial t^2},\quad \nabla^2\Psi=0,\quad \nabla^2\Phi=0 \tag{8}$$

where $E_{i,j}$ and $H_{i,j}$ denote the partial differentiation of $E_{i,j}$ and $H_{i,j}$ with respect to the corresponding coordinate variables x_j, respectively; $\nabla^2=\partial^2/\partial x_1^2+\partial^2/\partial x_2^2$ is a two-dimensional Laplace operator, and c_s is the speed of the stiffened bulk shear wave in the PE and/or PM materials given as

$$c_s=\sqrt{\frac{E_{11}}{\rho}} \tag{9}$$

Since the problem is in a steady state, the Galilean transformation can be introduced, i.e., $x=x_1-Vt$, $y=x_2$, $z=x_3$, where V is the speed of the crack tip, and then Eq. (8) can be rewritten as

$$\beta^2\frac{\partial^2 w}{\partial x^2}+\frac{\partial^2 w}{\partial y^2}=0,\quad \frac{\partial^2\Psi}{\partial x^2}+\frac{\partial^2\Psi}{\partial y^2}=0,\quad \frac{\partial^2\Phi}{\partial x^2}+\frac{\partial^2\Phi}{\partial y^2}=0 \tag{10}$$

where $\beta=\sqrt{1-V^2/c_s^2}$.

The general solution to Eq. (10) can be given as

$$\mathbf{U}=\left[w,\ \Psi,\ \Phi\right]^{\mathrm{T}}=\mathrm{Im}\left[\mathbf{f}\left(z\right)\right] \tag{11}$$

where $\mathbf{f}(z)=\left[f_1(z_1),\ f_2(z),\ f_3(z)\right]^{\mathrm{T}}$ and $z_1=x+\mathrm{i}\beta y$, $z=x+\mathrm{i}y$ and i is the imaginary number $\sqrt{-1}$. The generalized stresses can be presented as:

$$\begin{Bmatrix}\sigma_{23}\\ E_1\\ H_1\end{Bmatrix}=\mathrm{Re}\left[\mathbf{C}\mathbf{f}'(z)\right],\quad \mathbf{C}=\begin{bmatrix}E_{11}\beta & \mathrm{i}F_{12} & \mathrm{i}F_{13}\\ -\mathrm{i}F_{12} & -E_{22} & 0\\ -\mathrm{i}F_{13} & 0 & -E_{33}\end{bmatrix} \tag{12}$$

$$\begin{Bmatrix}\sigma_{31}\\ E_2\\ H_2\end{Bmatrix}=\mathrm{Im}\left\{\begin{bmatrix}E_{11} & -\mathrm{i}F_{12} & -\mathrm{i}F_{13}\\ \mathrm{i}\beta F_{12} & E_{22} & 0\\ \mathrm{i}\beta F_{13} & 0 & E_{33}\end{bmatrix}\mathbf{f}'(z)\right\} \tag{13}$$

For conductive cracks loaded by an electrical and/or magnetic field parallel to the crack, electric charges in the conductive crack surfaces will rearrange themselves to develop an opposite field with the same magnitude, therefore, the electric field and/or magnetic inside the conductive crack remains zero [15, 16]. As previously mentioned, the bimaterial is loaded by the anti-plane shear stress σ_0 as well as in-plane electric field E_0 and magnetic field H_0 parallel to crack line at infinity. According to the superposition principle, the problem here can be regarded as the sum of a uniform MEE field in PE/PM bimaterials with no cracking, and a disturbed MEE field caused by the moving conductive crack. The boundary and continuity conditions for the disturbed MEE field can be determined with

$$\begin{cases}\sigma_{32}\left(x,0^+\right)=\sigma_{32}\left(x,0^-\right)=-\sigma_0,\quad E_1\left(x,0^+\right)=E_1\left(x,0^-\right)=-E_0,\\ H_1^{(1)}\left(x,0^+\right)=H_1^{(2)}\left(x,0^-\right)=-H_0,\end{cases}\qquad |x|<a \tag{14}$$

$$\begin{cases}\sigma_{32}\left(x,0^+\right)=\sigma_{32}\left(x,0^-\right),\quad w\left(x,0^+\right)=w\left(x,0^-\right),\\ E_1\left(x,0^+\right)=E_1\left(x,0^-\right),\quad H_1\left(x,0^+\right)=H_1\left(x,0^-\right),\quad |x|\ge a\\ D_2\left(x,0^+\right)=D_2\left(x,0^-\right),\quad B_2\left(x,0^+\right)=B_2\left(x,0^-\right),\end{cases} \tag{15}$$

$$\sigma_{31}=\sigma_{32}=0,\quad D_1=D_2=0,\quad B_1=B_2=0,\quad z\to\infty \tag{16}$$

where superscripts ‘‘+’’ and ‘‘-’’ denote the physical quantities that pertain to the upper and the lower material interfaces, respectively.

3. MEE solution to the disturbed field

The continuity conditions of tractions, and the tangential electric and magnetic fields across the total real axis can be expressed as

$$\mathbf{C}_1\mathbf{f}_1'^{+}(x)+\bar{\mathbf{C}}_1\bar{\mathbf{f}}_1'^{-}(x)=\mathbf{C}_2\mathbf{f}_2'^{-}(x)+\bar{\mathbf{C}}_2\bar{\mathbf{f}}_2'^{+}(x),\quad -\infty<x<\infty \tag{17}$$

where subscripts 1 and 2 stands for the upper and lower materials, respectively; the prime $(')$ denotes differentiation with respect to the argument, the overbar stands for the complex conjugate; and

$$\bar{\mathbf{f}}_2'(z)=\bar{\mathbf{C}}_2^{-1}\mathbf{C}_1\mathbf{f}_1'(z),\quad \bar{\mathbf{f}}_1'(z)=\bar{\mathbf{C}}_1^{-1}\mathbf{C}_2\mathbf{f}_2'(z) \tag{18}$$

can be further obtained.

According to the continuity conditions of the out-of-plane displacement, normal electric displacement and magnetic induction on the bonded part of the material interface, we have

$$\mathbf{f}_1'^{+}(x)-\bar{\mathbf{f}}_1'^{-}(x)=\mathbf{f}_2'^{-}(x)-\bar{\mathbf{f}}_2'^{+}(x),\quad |x|\geq a \tag{19}$$

Substituting Eq. (18) into (19) yields:

$$\left(\mathbf{C}_1^{-1}+\bar{\mathbf{C}}_2^{-1}\right)\mathbf{C}_1\mathbf{f}_1'^{+}(x)=\left(\bar{\mathbf{C}}_1^{-1}+\mathbf{C}_2^{-1}\right)\mathbf{C}_2\mathbf{f}_2'^{-}(x),\quad |x|\geq a \tag{20}$$

Introducing an auxiliary function vector $\mathbf{h}(z)$ as in [17]:

$$\mathbf{h}(z)=\begin{cases}\mathbf{M}\mathbf{C}_1\mathbf{f}_1'(z), & y>0\\ \bar{\mathbf{M}}\mathbf{C}_2\mathbf{f}_2'(z), & y<0\end{cases} \tag{21}$$

where

$$\mathbf{M}=\mathbf{C}_1^{-1}+\bar{\mathbf{C}}_2^{-1}=\begin{bmatrix}M_{11} & \mathrm{i}M_{12} & \mathrm{i}M_{13}\\ -\mathrm{i}M_{12} & M_{22} & 0\\ -\mathrm{i}M_{13} & 0 & M_{33}\end{bmatrix} \tag{22}$$

with M_{ij} in (22) being real numbers. Using Eqs. (20) and (21), one gets

$$\mathbf{h}^{+}(x)-\mathbf{h}^{-}(x)=\mathbf{0},\quad |x|\geq a \tag{23}$$

$$\mathbf{h}(x)=\mathbf{0},\quad x\to\infty \tag{24}$$

Using the introduced function vector, the traction and tangential electric and magnetic fields on the crack surface in Eq. (14) can be expressed as

$$\mathbf{M}^{-1}\mathbf{h}^{+}(x)+\bar{\mathbf{M}}^{-1}\mathbf{h}^{-}(x)=2\mathbf{T},\quad |x|<a \tag{25}$$

where $\mathbf{T}=\left[-\sigma_0,\quad E_0,\quad H_0\right]^{\mathrm{T}}$. Eqs. (23)-(25) comprise a Riemann-Hilbert boundary value problem [22].

The aforementioned Riemann-Hilbert boundary value problem leads to the following eigenvalue problem and the details of the derivation can be found in Refs. [22-25]:

$$\left(\bar{\mathbf{H}}+e^{-2\pi i\delta}\mathbf{H}\right)\mathbf{v}=0 \tag{26}$$

where $\mathbf{v}$ is the eigenvector of the matrix $\left(\bar{\mathbf{H}}+e^{-2\pi i\delta}\mathbf{H}\right)$, and $\mathbf{H}=\mathbf{M}^{-1}$. With reference to [4], and by expressing $\mathbf{H}$ as $\mathbf{H}=\mathbf{D}+\mathrm{i}\mathbf{W}$, Eq. (26) further leads to

$$\left(\mathbf{\Psi}+\mathrm{i}\gamma\mathbf{I}\right)\mathbf{v}=0 \tag{27}$$

where

$$\mathbf{\Psi}=\mathbf{D}^{-1}\mathbf{W}=\begin{bmatrix}0 & \Psi_{12} & \Psi_{13}\\ \Psi_{21} & 0 & 0\\ \Psi_{31} & 0 & 0\end{bmatrix},\quad \gamma=\frac{1+e^{-2\pi\mathrm{i}\delta}}{1-e^{-2\pi\mathrm{i}\delta}} \tag{28}$$

and Ψ_{ij} are real. Then γ can be determined from $\left\|\mathbf{\Psi}+\mathrm{i}\gamma\mathbf{I}\right\|=0$ as

$$\gamma_{1,2}=\pm\sqrt{-\Psi_{12}\Psi_{21}-\Psi_{13}\Psi_{31}},\quad \gamma_3=0 \tag{29}$$

and δ can be further obtained by using the second equation of Eq. (28). According to Eqs. (12), (22), (28), and (29), δ is very dependent on the speed of the moving crack. With variations in the speed of the moving crack, the transitions of singularities will occur at the Rayleigh wave speeds of the upper and lower materials, as well as other speeds V_i that lie in between the

Rayleigh wave and the minimum shear wave speeds of the bimaterial system [17]. Therefore, the singularity parameters may take the three following forms for specific values of V .

(1) Case 1: $\delta_{1,2} = -\frac{1}{2} \pm \mathrm{i}\varepsilon, \quad \delta_3 = -\frac{1}{2}, \quad \text{for } 0 < -\Psi_{12}\Psi_{21} - \Psi_{13}\Psi_{31} < 1$

and

$$\varepsilon = \frac{1}{\pi}\operatorname{arccoth}\left(\gamma_1\right) + \frac{\mathrm{i}}{2} \tag{30}$$

This case usually occurs in regions of low speed. In this case, vector functions $\mathbf{f}_i'(z)$ and $\mathbf{f}_i(z)$ can be obtained by using the following derivation.

The transformation matrices are introduced:

$$\mathbf{h}(z) = \mathbf{P}\hat{\mathbf{h}}(z), \quad \hat{\mathbf{T}} = \boldsymbol{\Delta}\bar{\mathbf{P}}^{\mathrm{T}}\mathbf{T} \tag{31}$$

where

$$\mathbf{P} = \begin{bmatrix} \mathbf{v}_1 & \mathbf{v}_2 & \mathbf{v}_3 \end{bmatrix}, \ \boldsymbol{\Delta} = \operatorname{diag}\begin{bmatrix} 1-\tanh(\pi\varepsilon) & 1+\tanh(\pi\varepsilon) & 1 \end{bmatrix} \tag{32}$$

and $\mathbf{v}_i$ is the eigenvector associated with eigenvalue δ_i in Eq. (26), $\mathbf{v}_2 = \bar{\mathbf{v}}_1$. Then Eq. (25) can be decoupled as:

$$\hat{\mathbf{h}}^{+}(x) + \boldsymbol{\Lambda}\hat{\mathbf{h}}^{-}(x) = \hat{\mathbf{T}}, \quad |x| < a \tag{33}$$

where $\boldsymbol{\Lambda} = \operatorname{diag}\begin{bmatrix} e^{-2\pi\varepsilon} & e^{2\pi\varepsilon} & 1 \end{bmatrix}$.

Consequently, the expression for $\mathbf{h}(z)$ can be written as

$$\mathbf{h}(z) = \mathbf{P}\left[\mathbf{I} - \mathbf{X}(z)\mathbf{L}\right]\left(\mathbf{I} + \boldsymbol{\Lambda}\right)^{-1}\hat{\mathbf{T}} \tag{34}$$

where

$$\mathbf{X}(z) = \operatorname{diag}\left[(z+a)^{-\frac{1}{2}-\mathrm{i}\varepsilon}(z-a)^{-\frac{1}{2}+\mathrm{i}\varepsilon} \quad (z+a)^{-\frac{1}{2}+\mathrm{i}\varepsilon}(z-a)^{-\frac{1}{2}-\mathrm{i}\varepsilon} \quad (z+a)^{-\frac{1}{2}}(z-a)^{-\frac{1}{2}} \right] \tag{35}$$

$$\mathbf{L} = \operatorname{diag}\begin{bmatrix} z + 2\mathrm{i}a\varepsilon & z - 2\mathrm{i}a\varepsilon & z \end{bmatrix} \tag{36}$$

Using Eq. (21), the explicit expressions for $\mathbf{f}_1(z)$ and $\mathbf{f}_2(z)$ are

$$\mathbf{f}_1'(z)=\mathbf{C}_1^{-1}\mathbf{M}^{-1}\mathbf{P}\left[\mathbf{I}-\mathbf{X}(z)\mathbf{L}\right](\mathbf{I}+\mathbf{\Lambda})^{-1}\widehat{\mathbf{T}} \tag{37a}$$

$$\mathbf{f}_2'(z)=\mathbf{C}_2^{-1}\bar{\mathbf{M}}^{-1}\mathbf{P}\left[\mathbf{I}-\mathbf{X}(z)\mathbf{L}\right](\mathbf{I}+\mathbf{\Lambda})^{-1}\widehat{\mathbf{T}} \tag{37b}$$

Integrating Eq. (37) gives

$$\mathbf{f}_1(z)=\mathbf{C}_1^{-1}\mathbf{M}^{-1}\mathbf{P}\left[z\mathbf{I}-\left(z^2-a^2\right)\mathbf{X}(z)\right](\mathbf{I}+\mathbf{\Lambda})^{-1}\widehat{\mathbf{T}} \tag{38a}$$

$$\mathbf{f}_2(z)=\mathbf{C}_2^{-1}\bar{\mathbf{M}}^{-1}\mathbf{P}\left[z\mathbf{I}-\left(z^2-a^2\right)\mathbf{X}(z)\right](\mathbf{I}+\mathbf{\Lambda})^{-1}\widehat{\mathbf{T}} \tag{38b}$$

(2) Case 2: $\delta_{1,2}=-1\pm\mathrm{i}\varepsilon,\quad \delta_3=-\dfrac{1}{2},\quad$ for $-\Psi_{12}\Psi_{21}-\Psi_{13}\Psi_{31}>1$

and

$$\varepsilon=\frac{1}{\pi}\operatorname{arc\,coth}(\gamma_1) \tag{39}$$

This case probably occurs with a moderate speed of the moving crack. In this case, $\mathbf{\Delta}$ in Eq. (32) and $\mathbf{\Lambda}$ in Eq. (33) will, respectively, become

$$\mathbf{\Delta}=\operatorname{diag}\left[-1+\coth(\pi\varepsilon)\quad -1-\coth(\pi\varepsilon)\quad 1\right],\quad \mathbf{\Lambda}=\operatorname{diag}\left[-e^{-2\pi\varepsilon}\quad -e^{2\pi\varepsilon}\quad 1\right] \tag{40}$$

and

$$\mathbf{h}(z)=\mathbf{P}\left[\mathbf{I}-\mathbf{X}(z)\mathbf{L}\right](\mathbf{I}+\mathbf{\Lambda})^{-1}\widehat{\mathbf{T}} \tag{41}$$

where

$$\mathbf{X}(z)=\operatorname{diag}\left[(z+a)^{-\mathrm{i}\varepsilon}(z-a)^{-1+\mathrm{i}\varepsilon}\quad (z+a)^{\mathrm{i}\varepsilon_2}(z-a)^{-1-\mathrm{i}\varepsilon}\quad (z+a)^{-\frac{1}{2}}(z-a)^{-\frac{1}{2}}\right] \tag{42}$$

$$\mathbf{L}=\operatorname{diag}\left[z+(2\mathrm{i}-1)a\varepsilon\quad z-(2\mathrm{i}+1)a\varepsilon\quad z\right] \tag{43}$$

Also, $\mathbf{f}_i'(z)$ and $\mathbf{f}_i(z)$ which are associated with this scenario are formally analogous to Eqs. (37) and (38), respectively. Unless otherwise stated, the quantities or symbols in this case as well as in the following cases will take the same form as those in Case 1.

(3) Case 3: $\delta_{1,2} = -\frac{1}{2} \pm \kappa, \quad \delta_3 = -\frac{1}{2}, \quad \text{for } -\Psi_{12}\Psi_{21} - \Psi_{13}\Psi_{31} < 0$

and

$$\varepsilon = -\frac{\mathrm{i}}{\pi}\operatorname{arccoth}\left(\gamma_1\right) + \frac{1}{2} \tag{44}$$

Correspondingly, $\mathbf{\Delta}$ and $\mathbf{\Lambda}$ in Eqs. (32) and (33) will, respectively, take the following form:

$$\mathbf{\Delta} = \begin{bmatrix} 0 & 0 & -1+\mathrm{i}\left[\tan\left(\kappa\pi\right)\right] \\ 0 & -1-\mathrm{i}\left[\tan\left(\kappa\pi\right)\right] & 0 \\ -1 & 0 & 0 \end{bmatrix}, \quad \mathbf{\Lambda} = \operatorname{diag}\left[e^{2\pi\mathrm{i}\kappa} \quad e^{-2\pi\mathrm{i}\kappa} \quad 1\right] \tag{45}$$

and

$$\mathbf{h}\left(z\right) = \mathbf{P}\left[\mathbf{I} - \mathbf{X}\left(z\right)\mathbf{L}\right]\left(\mathbf{I} + \mathbf{\Lambda}\right)^{-1}\hat{\mathbf{T}} \tag{46}$$

where

$$\mathbf{X}\left(z\right) = \operatorname{diag}\left[\left(z+a\right)^{-\frac{1}{2}-\kappa}\left(z-a\right)^{-\frac{1}{2}+\kappa} \quad \left(z+a\right)^{-\frac{1}{2}+\kappa}\left(z-a\right)^{-\frac{1}{2}-\kappa} \quad \left(z+a\right)^{-\frac{1}{2}}\left(z-a\right)^{-\frac{1}{2}}\right] \tag{47}$$

$$\mathbf{L} = \operatorname{diag}\left[z+2a\kappa \quad z-2a\kappa \quad z\right] \tag{48}$$

Likewise, $\mathbf{f}_i'\left(z\right)$ and $\mathbf{f}_i\left(z\right)$ in relation to this scenario are analogous to Eqs. (37) and (38), respectively.

The exact solutions derived in the previous section can be readily applied to determine the field variables at the material interface.

5. Numerical results of singularity and discussion

In this section, the effect of the speed of the moving crack on different singularity powers will be numerically examined and discussed. Two bimaterial combinations with PE and PM solids, i.e., $BaTiO_3/CoFe_2O_4$ and $BaTiO_3$/Terfenol-D, are considered. For convenience, their material properties are listed in Table 1 [26]. The explicit expression of Rayleigh wave speed of the PM

or PE material is not available and its calculation methodology can be found in Feng et al. [27]. Herein Rayleigh wave speeds for $BaTiO_3$, $CoFe_2O_4$ and Terfenol-D are, respectively, 3031.72 m/s, 2939.87 m/s, 1293.35 m/s, and their shear wave speeds are, respectively, 3106.71 m/s, 2940.05m/s, 1305.79 m/s. Since δ_3 always equals to $-1/2$ in all three cases in Section 3, only the results in relation to $\delta_i\,(i=1,2)$ are provided herein.

Table 1 Material properties of $BaTiO_3$, $CoFe_2O_4$ and Terfenol-D [26]

(c_{ij} in 10^9 N/m^2, e_{ij} in C/m^2, α_{ij} in 10^{-10}C/Vm, h_{ij} in N/Am, μ_{ij} in 10^{-6}Ns^2/ C^2, d_{ij} in 10^{-12}Ns/ VC, ρ in kg/m^3)

	c_{44}	e_{15}	h_{15}	α_{11}	μ_{11}	d_{11}	ρ
$BaTiO_3$	43	11.6	0	112	5	0	5700
$CoFe_2O_4$	45.3	0	550	0.8	590	0	5300
Terfenol-D	13.6	0	108.3	0.5	5.4	0	9250

Figs. 2 and 3 describe the variations in the oscillating index ε with respect to the speed of the moving crack for the bimaterial systems of $BaTiO_3/CoFe_2O_4$ and $BaTiO_3$/Terfenol-D, respectively. Note that in Fig.2, there is one transition point of the singularities at the Rayleigh wave speed of $CoFe_2O_4$, i.e., V=2939.87 m/s, for the $BaTiO_3/CoFe_2O_4$ bimaterial system. When the speed of the moving crack V exceeds 2939.87 m/s, the singularity indexes change from $\delta_{1,2}=-1/2\pm \mathrm{i}\varepsilon$ (Case 1) to $\delta_{1,2}=-1\pm \mathrm{i}\varepsilon$ (Case 2). Fig. 3 shows that there are two points of transition of the singularities for the bimaterial system of $BaTiO_3$/Terfenol-D, in which one of the points is at the Rayleigh wave speed of Terfenol-D, namely V=1293.35 m/s, and the other point is at a speed of V_1=1302.92 m/s, which lies in between the Rayleigh wave and shear wave speeds of Terfenol-D. The singularity parameters which are defined as $\delta_{1,2}=-1/2\pm \mathrm{i}\varepsilon$ (Case 1), $\delta_{1,2}=-1\pm \mathrm{i}\varepsilon$ (Case 2) and $\delta_{1,2}=-1/2\pm\kappa$ (Case 3) for the bimaterial system of

$BaTiO_3$/Terfenol-D, appear successively with increased speed of the moving crack. The results in Figs. 2a and 3a show that for the majority of the range $0 < V < \min\left(c_{\mathrm{R}}^{(1)}, c_{\mathrm{R}}^{(2)}\right)$, where c_{R} is Rayleigh wave speed, increasing the speed of the moving crack leads to an increase in the oscillating index. Moreover, when the speed of the moving crack is close to the minimum Rayleigh wave speed of the system, the oscillating index increases rapidly and approaches to infinity. These phenomena agree with the findings of the analysis on anti-plane fractures of moving conductive cracks in piezoelectric bimaterials [17] and plane fracture analysis of permeable moving interface cracks in MEE bimaterials [12]. Figs. 2b and 3b show that in the event that Case 2 occurs, namely $\delta_{1,2} = -1 \pm \mathrm{i}\varepsilon$, the magnitude of the oscillating index decreases as the speed of the moving crack increases. This is also consistent with the observations in [17]. However, for the bimaterial system of $BaTiO_3/CoFe_2O_4$, only Cases 1 and 2 appear, and Case 3, namely the real singularity parameter, vanishes. This is not consistent with the observation in [17], which is probably owing to the material properties of bimaterial system of $BaTiO_3/CoFe_2O_4$.

In Fig. 3b, as the speed of the moving crack is greater than V_1=1302.92 m/s, all of the singularity parameters become real, which means that the oscillation vanishes. In short, the numerical results shown in Figs. 2 and 3 indicate that the speed of the moving crack significantly influences the singularity parameters of the piezoelectric/piezomagnetic bimaterials in this study. The anti-plane moving interface crack model including impermeable and permeable crack-face assumptions leads to the inverse square root singularity [28], while the current model leads to 3 kinds of singularities as the speed of the moving crack changes. This is probably owing to the crack-face boundary conditions used in this study where the electric field and/or magnetic inside the conductive crack remains zero. This could result in a quite different distribution of magnetoelectroelastic field especially for a relative high the speed of the moving crack.

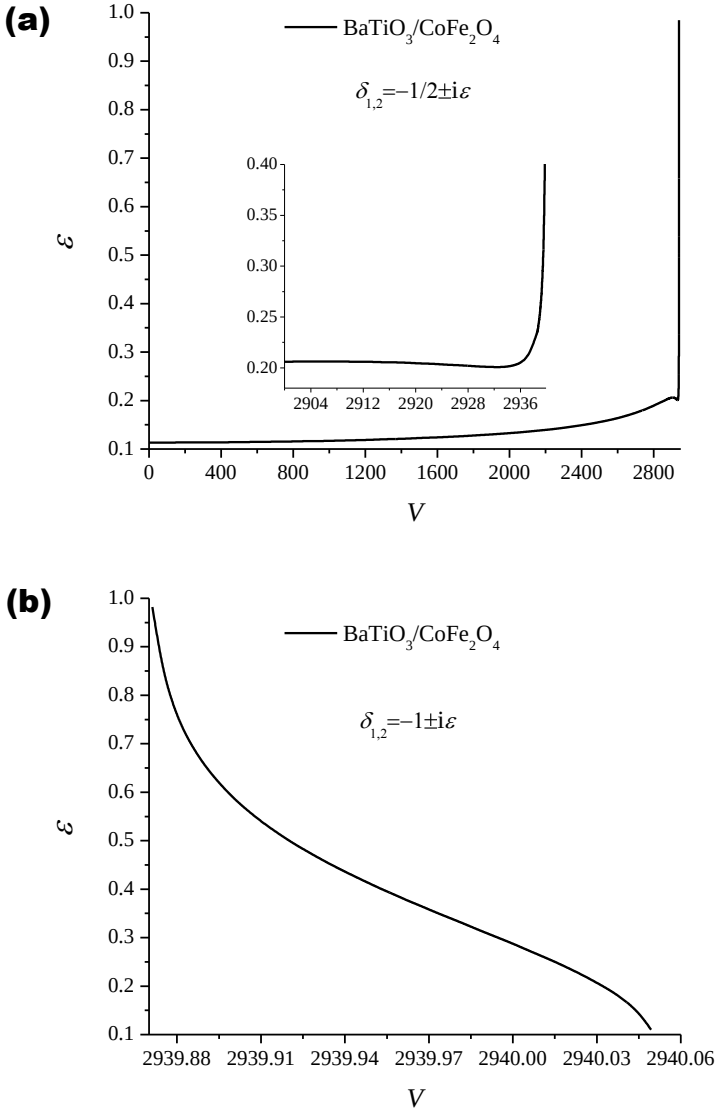

Fig. 2. Variations in oscillation index ε with respect to speed of moving crack for bimaterial system of $BaTiO_3/CoFe_2O_4$ which range from (a) $0 < V < \min\left(c_R^{(1)}, c_R^{(2)}\right)$, to (b) $\min\left(c_R^{(1)}, c_R^{(2)}\right) < V < \min\left(c_s^{(1)}, c_s^{(2)}\right)$

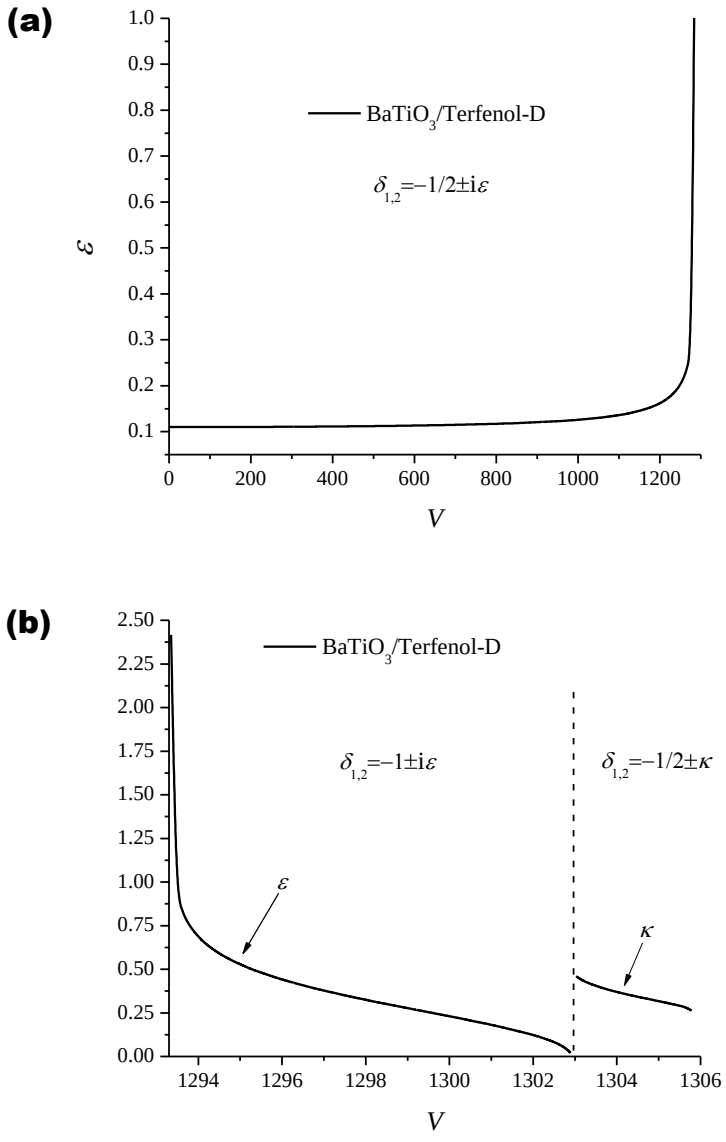

Fig. 3. Variations in ε and κ with respect to speed of moving crack for bimaterial system of $BaTiO_3$/Terfenol-D which range from (a) $0 < V < \min\left(c_{\mathrm{R}}^{(1)}, c_{\mathrm{R}}^{(2)}\right)$, to (b) $\min\left(c_{\mathrm{R}}^{(1)}, c_{\mathrm{R}}^{(2)}\right) < V < \min\left(c_{\mathrm{s}}^{(1)}, c_{\mathrm{s}}^{(2)}\right)$

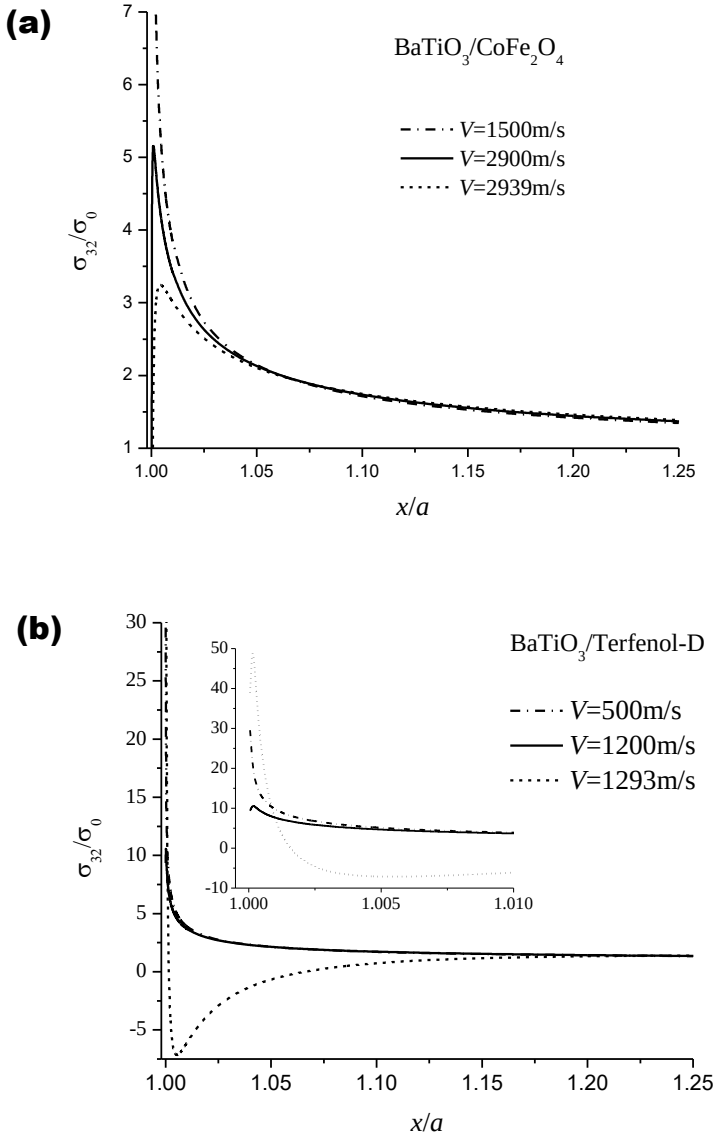

Fig. 4. Distribution of the stress ahead of the moving crack-tip for different speeds of moving cracks. Bimaterial system of (a) $BaTiO_3/CoFe_2O_4$, and (b) $BaTiO_3$/Terfenol-D

The distribution of the stress ahead of the moving crack-tip for different speeds of moving cracks is presented in Fig. 4. Herein, the applied external loading is expressed as $\mathbf{T}=\{-\sigma_0,\ 0,\ 0\}^{\mathrm{T}}$. It should be noted that the stress oscillation becomes more obvious when the speed of the moving crack is close to the Rayleigh wave speed of $CoFe_2O_4$ and Terfenol-D, respectively. As expected, stress is rapidly reduced beyond the oscillation interval and finally

tends to a constant value with increases in x/a, which is consistent with the observation in [17]. However, for $BaTiO_3$/Terfenol-D material combination, the stress ahead of the moving crack-tip is negative for a very high speed of moving crack. This is different from the phenomena in [17] for piezoelectric bimaterial, which is probably owing to the special material properties of $BaTiO_3$/Terfenol-D material combination.

6. Conclusions

A Yoffe conductive crack moving along the interface of PE/PM bimaterials is analyzed by using the complex variable method. By assuming the moving speed is less than the minimum shear wave speed of the bimaterial system, the problem can be reduced to solving a Riemann-Hilbert boundary value problem in vector form, the solution to which is given in closed form. The singularity parameters for the crack model are obtained for different speed regions. It is found that as the moving speed increases, three different kinds of singularities may emerge in this study, namely $\delta_{1,2} = -1/2 \pm \mathrm{i}\varepsilon$ (Case 1), $\delta_{1,2} = -1 \pm \mathrm{i}\varepsilon$ (Case 2) and $\delta_{1,2} = -1/2 \pm \kappa$ (Case 3), and that $\delta_3 = -1/2$ always holds true for all cases. Moreover, the transitions of singularities usually occur at the minimum Rayleigh wave speed of the two constituents or at certain speeds that fall in between the minimum Rayleigh wave and shear wave speeds. Different from the piezoelectric case, Case 3 does not appear for $BaTiO_3/CoFe_2O_4$ bimaterial combination. As for $BaTiO_3$/Terfenol-D bimaterial combination, all three cases occur. Additionally, the singularity parameters significantly depend on the speed of the moving crack and the material properties of bimaterial systems.

Acknowledgement

Support from the General Research Fund of Hong Kong (HKU 17223916), the National Natural Science Foundation of China (Grant Nos. 11572358 , 10772123 and11072160) and the

Training Program for Leading Talent in University Innovative Research Team in Hebei Province (LJRC006) is gratefully acknowledged.

References

[1] Nan C.W., Bichurin M.I., Dong S.X., Viehland D., Srinivasan G.： Multiferroic magnetoelectric composites: historical perspective, status, and future directions. J. Appl. Phys. 103, 031101 (2008) .

[2] Chen H.S., Wei W.Y., Liu J.X., Fang D.N.: Propagation of a Mode-III interfacial crack in a piezoelectric-piezomagnetic bi-material. Int. J. Solids Struct. 49, 2547-2558 (2012).

[3] Li Y.D., Zhao H., Zhang N.：Mixed mode fracture of a piezoelectric-piezomagnetic bi-layer structure with two un-coaxial cracks parallel to the interface and each in a layer. Int. J. Solids Struct. 50, 3610-3617 (2013).

[4] Shen S., Nishioka T., Hu S.L.: Crack propagation along the interface of piezoelectric bimaterial. Theor. Appl. Fract. Mech. 34, 185-203 (2000).

[5] Zhou K., Liu S.L., Li Y.D.: Effects of the volume fraction of piezoelectric particles in the magneto-electro-elastic interfacial region on the fracture behavior of a laminate multiferroic plate. Acta Mech. 228, 1229-1248 (2017).

[6] Zhou Z.G., Zhou P.W., Wu L.Z.: Basic solutions of a 3D rectangular limited-permeable crack or two 3D rectangular limited-permeable cracks in the piezoelectric/piezomagnetic composite materials. Appl. Math. Model. 36, 2404-2428 (2012).

[7] Yoffe E.H.: The moving Griffith crack. Philos. Mag. 42, 739-750 (1951) .

[8] Fang D.N., Liu J.X.: Fracture mechanics of piezoelectric and ferroelectric solids, Berlin: Springer-Verlag, 2012.

[9] Zhong X.C., Li X.F.: A finite length crack propagating along the interface of two dissimilar magnetoelectroelastic materials. Int. J. Eng. Sci. 44, 1394-1407 (2006) .

[10] Hu K., Chen Z.: An interface crack moving between magnetoelectroelastic and functionally graded elastic layers. Appl. Math. Model. 38, 910-925 (2014).

[11] Hu K., Chen Z., Fu J.: Moving Dugdale crack along the interface of two dissimilar magnetoelectroelastic materials. Acta Mech. 226, 2065-2076 (2015).

[12] Ma P., Su R.K.L., Feng W.J.: Moving crack with a contact zone at interface of magnetoelectroelastic bimaterial. Eng. Fract. Mech. 181, 143-160 (2017).

[13] Fu R., Qian C.F., Zhang T.Y.: Electric fracture toughness for conductive cracks driven by electric fields in piezoelectric materials. Appl. Phys. Lett. 76, 126-128 (2000).

[14] Wang T., Zhang T.Y.: Electric fracture toughness for conductive deep notches driven by electric fields in depoled lead zirconate titanate ceramics. Appl. Phys. Lett. 79, 4198-4200 (2001).

[15] Tian W.Y., Rajapakse R.K.N.D.: Theoretical modelling of a conducting crack in a magnetoelectroelastic solid. Int. J. Appl. Electrom. Mech. 22, 141-158 (2005).

[16] Ma P., Su R.K.L., Feng W.J.: Fracture analysis of an electrically conductive interface crack with a contact zone in a magnetoelectroelastic bimaterial system. Int. J. Solids Struct. 53, 48-57 (2015).

[17] Wang X., Zhong Z., Wu F.L.: A moving conducting crack at the interface of two dissimilar piezoelectric materials. Int. J. Solids Struct. 40, 2381-2399 (2003).

[18] Wang Y.Z.: Effects of Maxwell stress on interfacial crack between two dissimilar piezoelectric solids. ASME J. Appl. Mech. 81, 101003 (2014).

[19] Zhang A.B., Wang B.L.: The influence of Maxwell stresses on the fracture mechanics of piezoelectric materials. Mech. Mater. 68, 64-69 (2014).

[20] Wang Y.Z.: Influences of the remanent polarization and Maxwell stress in surrounding medium on a moving anti-plane crack between two dissimilar piezoelectric solids. Theor. Appl. Fract. Mech. 80, 253-258 (2015).

[21] Wang Y.Z.: Influences of imperfect interface on effective magnetoelectric properties in multiferroic composites with elliptical fibers. Smart Mater. Struct. 24, 045021 (2015).

[22] Wang X., Zhong Z.: A conducting arc crack between a circular piezoelectric inclusion and an unbounded matrix. Int. J. Solids Struct. 39, 5895-5911 (2002).

[23] Suo Z.G., Kuo C.M., Barnett D.M.: Fracture mechanics of piezoelectric ceramics. J. Mech. Phys. Solids 40, 739-765 (1992).

[24] Li R., Kardomateas G.A.: The mixed Mode I and II interface crack in piezoelectromagneto–elastic anisotropic bimaterials. ASME J. Appl. Mech. 74, 614-627 (2007).

[25] Fang D., Liu J.: Fracture Mechanics of Piezoelectric and Ferroelectrics Solids. Berlin: Springer-Verlag, 2012.

[26] Kuo H.Y., Pan E.: Effective magnetoelectric effect in multicoated circular fibrous multiferroic composites. J. Appl. Phys. 109, 104901 (2011).

[27] Feng W.J., Pan E., Wang X., Liu J.X.: Rayleigh waves in magneto-electro-elastic half planes. Acta Mech. 202, 127-134 (2009).

[28] Hu K.Q., Kang Y.L., Li G.Q.: Moving crack at the interface between two dissimilar magnetoelectroelastic materials. Acta Mech. 182, 1-16 (2006).